Dragon 4 – Satellite based analysis of diseases on permanent and row crops in Italy and China

LANEVE Giovanni[1*], LUCIANI Roberto[2], MARZIALETTI Pablo[2], PIGNATTI Stefano[3], HUANG Wejiang, SHI Yue , DONG YingYing , YE Huichun , Scuola di Ingegneria Aerospaziale [1,2,3], Sapienza Università di Roma[1,2,3], Roma[1,2,3], Italy[1,2,3], roberto.luciani@uniromait

1. *DIAEE, Sapienza Università di Roma, Italy*;
2. *IMAA – CNR, Roma Italy*;
3. *RADI, Chinese Academy of Sciences, Beijing, China*

Abstract: A The AMEOS (Assimilating Multi-source Earth Observation Satellite data for crop pests and diseases monitoring and forecasting) project aims to bring together cutting edge research to provide pest and disease monitoring and forecast information, integrating multi-source information (Earth Observation, meteorological, entomological and plant pathological, etc.) to support decision making in the sustainable management of insect pests and diseases in agriculture. The main objective of the project, that is, improving crop diseases and pests monitoring and forecasting, will be achieved by utilizing EO data, developing new algorithms, and combining new and existing data from multi-source EO sensors to produce high spatial and temporal land surface information. The project foresees the assessment of the possibility of using available satellite images datasets to assess the evolution of diseases on permanent (olive groves, vineyards), or row crops (wheat) in Italy and China. The paper describes the results of the research activity which focused on: (i) improving the classification of the agricultural areas devoted to winter wheat and olive trees, starting from what has been made available from the Corine Land Cover initiative; (ii) developing an approach suitable to be automated for estimating trees by using Sentinel 2 images; (iii) developing a new index, REDSI (consisting of Red, Re_1, and Re_3 bands), for detecting and monitoring yellow rust infection of winter wheat at the canopy and regional scale. The research activity covers the: 1) Province of Lecce, that is the Italian area strongly affected, since 2015, by the Xylella fastidiosa disease which causes a rapid decline in olive plantations. 2) Province of Anyang, Neihuang county, which was affected by the yellow rust disease in the spring 2017.

Key words: Disease, reflectance, index, morphology, classification

Citation format: Laneve G,Luciani R,Marzialetti P,Pignatti S,Huang W J,Shi Y,Dong Y Y,Ye H C, Scuola di Ingegneria Aerospaziale and Sapienza Università di Roma. 2020. Dragon 4 – Satellite based analysis of diseases on permanent and row crops in Italy and China. Journal of Remote Sensing(Chinese). 24(S1): 39–49

1 INTRODUCTION

The AMEOS project aims to develop innovative EO based solutions to crop diseases and pests monitoring and forecasting based on the complementary expertise of Chinese, Italian research groups in remote sensing, plant protection and data assimilation through integrating multi-source information (Earth Observation-EO, meteorological, entomological and plant pathological, etc.) to support decision making in the sustainable management of insect pests and diseases in agriculture. The main objective of this project is to ensure food security by improving crop diseases and pests monitoring and forecasting. This will be achieved through the utilization of EO data, the development of new algorithms, and the fusion of new and existing data products using multi-source data to develop innovative methods for crop pests and diseases monitoring and forecasting at regional level, with a fungal disease of wheat (stripe rust), a serious insect pest (ostrinia nubilalis) of maize and an olive groves threat (xylella fastidiosa) [1-3], as examples. The specific objectives covers:

(1) Multi-source space- and ground-based remote sensing data integration, processing and scale transformation. The research will focus on processing of near synchronously acquired various satellite- and ground-based re-motely sensed data, assimilation of multi-source satellite data of various spatial resolution based on scale transformation technique, thus providing a high spatial and temporal resolution datasets for crop diseases and pests monitoring and forecasting.

(2) Research on crop diseases and pests monitoring with new-launched satellite data. Based on the assimilated remote sensing data, the team will study the spectral response of stripe rust in winter

Received: 2019-10-21; **Accepted:** 2020-04-26
Corresponding author biography: giovanni.laneve@uniroma1.it

wheat, ostrinia nubilalis in maize and xylella fastidiosa in olive trees, analyze these spectral features, and establish monitoring methods through integrating spectral, temporal and landscape features of satellite date to better monitor diseases and pests in the early stage.

(3) Crop diseases and pests habitat factors retrieval through integrating multi-source data. With the help of GIS, geostatistics and data fusion techniques, the research team will focus on the key parameters for characterizing the habitat through integrating multi-source information (Earth Observation, meteorological, entomological and plant pathological, etc.), study the methods for key habitat factors accurate extraction and retrieval, and provide basic information for diseases and pests forecasting.

(4) Study on crop diseases and pests forecasting through assimilating multi-source information. Based on the diseases and pests' prevalence mechanism and dispersal pattern, assimilated multi-source datasets and retrieved habitat factors, the project will integrate these information to establish robust forecasting models for crop diseases and pests monitoring at regional scale.

(5) Crop diseases and pests monitoring and forecasting for applied research and demonstration. Based on the above methods and techniques, the research team is conducting crop diseases and pests monitoring and forecasting for applied research and demonstration in North central plain in China constituting five provinces Hebei, Shandong, Henan, Jiangsu and Anhui and South-Italy (Apulia region). Through applied research and demonstration, the research will take advantage of newly multi-source EO data and assimilation techniques to acquire re-al-time crop diseases and pests information at regional scale to support decision-making in agricultural management.

The outcomes of the project will not only promote efficacy of pests and diseases management and prevention by improving the accuracy of monitoring and forecasting, but also help to reduce the amount of chemical pesticides, with better management of pests and diseases will achieve increase in production and in turn ensure food security.

The explicit quantification of vegetation biophysical variables on large spatial scales is an important aspect in agricultural management and monitoring [4]. Remotely sensed data from satellites and airborne sensors has great potential to provide information on vegetation biophysical variables (LAI, leaf area index, chlorophyll content, water content, temperature) over large spatial and temporal scales [5].

Plant diseases and pests can affect a wide range of commercial crops, and result in a significant yield loss. It is reported that at least 10% of global food production is lost due to plant diseases [6-7]. Disease and pest control could be more efficient if disease and pest patches within fields can be identified timely and treated locally. Remote sensing technology can provide spatial distribution information of diseases and pests over a large area at relatively low cost. The presence of diseases or insect feedings on plants or canopy surface causes changes in pigment, chemical concentrations, cell structure, nutrient, water uptake, and gas exchange [8]. These changes result in differences in spectral reflectance characteristics and temperature of the canopy which can be detectable by remote sensing [9].

Therefore, remote sensing provides a harmless, rapid, and cost-effective means of identifying and quantifying crop stress from differences in the spectral characteristics of canopy surfaces affected by biotic and abiotic stress agents.

During the last decades, scientific publications have described the capability and potential of RS approaches for plant disease detection. See Martinelli [10] for a review. The RS scientific community defines plant disease monitoring as: detection (deviation from healthy), identification (diagnosis of specific symptoms among others and differentiation of various diseases), and quantification (measurement of disease severity, e.g., percent leaf area affected) [11]. Different sensors and techniques are required for detecting plant response to various diseases and disease severity. The ability of RS to diagnose plant disease and severity are shown in works describing the application of multispectral, hyperspectral and thermal imagery for detecting disease in almond orchards [12] or barley, wheat and sugar beet [13] or tomato plants [14] or apple trees [15] or pine [16], etc. [17].

This paper is devoted to describe the achievement of the DRAGON-4 AMEOS project in detecting and discriminating yellow rust and xylella fastidiosa (economically important disease and pest in winter wheat in China and olive groves in Italy) by using field and satellite remote sensing.

2 Materials and Methods

2.1 Materials

2.1.1 Italian test site

The area of interest is shown in Fig. 1. It corresponds to the Province of Lecce, located in the Southern part of the Apulia Region. 77 Sentinel-2 (MSI) cloud free images of the area of interest covering the period February 2015 – July 2017, were found in the ESA database (tale T33XE). The list of images is given in Table 1.

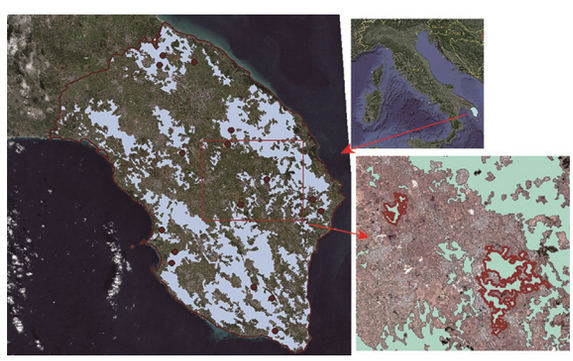

Fig.1 Area of Interest. On left the Province of Lecce is shown with, in grey, the distribution of olive groves, according to CORINE Land Cover (CLC) 2012 map. In red some of the points analyzed by the local authorities to monitor the presence of the disease. On the right, in red are shown the two CLC 223 polygons selected for illustrating the results of the analysis (see following paragraphs).

A Very High spatial Resolution (VHR) acquired by the GaoFen1 Chinese satellite was obtained through RADI. The characteristics of the EO sensor on board of such satellite are given in Table 2.

To validate the proposed approach only the part of the Lecce Province covered by both S2A and S2B images has been considered. Therefore, the actual area interested by the analysis has been shown in Fig. 2, together with the map showing the point where the tests for detecting the presence of the diseases have been carried out by the local authorities.

The area of interest is shown in Fig. 3. Two Sentinel-2 multispectral images were acquired on 12 May 2017, fromhttps://scihub.copernicus.eu/, and the full coverage image was mosaicked by these two images acquired simultaneously. Atmospheric correction for the Sentinel-2 images was conducted based on the Sen2cor atmospheric correction toolbox in the SNAP (Sentinel Application Platform) software. The spatial resolution of all bands was resampled up to 10 m for subsequent analysis. The coastal aerosol (B1),

water vapor (B9), and cirrus (B10) bands were removed from the study due to their irrelevance. A ground survey was conducted on 9 May 2017, and 27 sample plots in the region were investigated. The size of each sample point was 10 m × 10 m, and five sampling subplots with a 1 m × 1 m in each plot (five-point sampling) were used to record the average severity. Each plot's central coordinates were collected using a Trimble GeoXT DGPS with submeter accuracy.

Table 1 List of Sentinel-2 images available for the analysis on area of interest in Italy

2015 (cont)	2016 (cont)	2016 (cont)	2017 (cont)	2017 (cont)	2017 (cont)
2015-07-15	2016-01-01	2016-11-13	2017-01-02	2017-06-14	2017-08-18
2015-07-25	2016-04-20	2016-11-23	2017-01-25	2017-06-21	2017-08-23
2015-08-01	2016-04-30	2016-12-03	2017-02-11	2017-06-24	2017-08-25
2015-08-14 (0 e 1)	2016-05-07	2016-12-16	2017-02-14	2017-07-01	2017-08-28
2015-08-24	2016-05-27	2016-12-26	2017-03-03	2017-07-04	2017-08-30
2015-08-31	2016-05-30	2016-11-13	2017-03-06	2017-07-06	2017-09-02
2015-09-13	2016-06-26		2017-03-16	2017-07-09	2017-09-12
2015-10-23	2016-06-29		2017-03-23	2017-07-11	2017-10-17
2015-12-09	2016-07-06		2017-04-12	2017-07-14	2017-10-27
2015-12-22	2016-07-09		2017-04-15	2017-07-19	2017-10-29
	2016-07-19		2017-05-02	2017-07-21	2017-12-06
	2016-07-29		2017-05-05	2017-07-24	2017-12-08
	2016-08-15		2017-05-22	2017-07-29	2017-12-23
	2016-08-25		2017-06-01	2017-07-31	2017-12-31
	2016-08-28		2017-06-04	2017-08-05	
	2016-10-14			2017-08-08	

Table 2 GF1 sensor characteristics.

	VHR Sensor	HR sensor
Main sensor characteristics	2 x HR (High Resolution Cameras)	4 x WFV(Wide field of view Cameras)
Spatial resolution	Pan: 2 m, MS: 8 m	MS: 16 m
Spectral resolution	Pan: 0.45—0.90 B1: 0.45—0.52 μm B2: 0.52—0.59 μm B3: 0.63—0.69 μm B4: 0.77—0.89 μm	B1: 0.45—0.52 μm B2: 0.52—0.59 μm B3: 0.63—0.69 μm B4: 0.77—0.89 μm
Swath width	69 km with 2 cameras	830 km with 4 cameras mosaic
Data quantization	10 bit	10 bit
Revisit capability	4 days at equator (roll needed)	4 days (no roll needed)

2.2. Methods

In a previous study of which a summary is reported in the DRAGON 2018 brochure [18] the possibility to detect olive groves affected by xylella and winter wheat affected by yellow rust were demonstrated by considering several fields and observing the behavior of the annual variation of the NDVI (Normalized Difference Vegetation In-dex) [19-20]. It is worthwhile to recall that olive trees present a reduced phenology all along the year. Therefore, unchanged and changed (eradicated) olive groves show a distinctive behavior due to the change caused by the trees eradication requested to stop the spread of the disease. In the plot where the olive trees have been eradicated the NDVISTDN increases significantly due to the reduced importance of the evergreen olive trees in determining the behavior of NDVI with respect to the background characterized by the presence of grass or shrub. NDVISTDN is the normalized standard deviation of NDVI computed by using all the images of the area of interest acquired during a calendar year.

However, this analysis was done on several plots selected taking into account the sites where the check of the pres-ence of the disease was carried out. As result of the inspection, in some cases it was not necessary to remove the plants, in other cases the olive plants were eradicated. The delineation of the plots was carried out manually by visual inspec-tion of the image. In fact, using the polygons taken from the 2012 CLC (Corine Land Cover, https://land.copernicus. eu/pan-european/corine-land-cover 2020-04-16) map which correspond to olive groves (CLC 223) was not effective since the variability of the surface cover within such polygons is very high, see Fig. 4 [21-22]. Thus, this paper focuses on the development of a technique suitable to identify olive groves with higher

accuracy than CLC. The classification has been carried out by using Sentinel-2 images. The methodology and its results are described below. However, olive groves are characterized by a significant variability in terms of tree den-sity and we are also interested in monitoring the number of trees for each field to be able to follow their change as consequence of the disease or the eradication intervention. The approach followed, and the hypothesis on which it is based, for counting the olive trees by using S2 images, and the fraction cover computed by using NDVI values range in each field has been also described in [18].

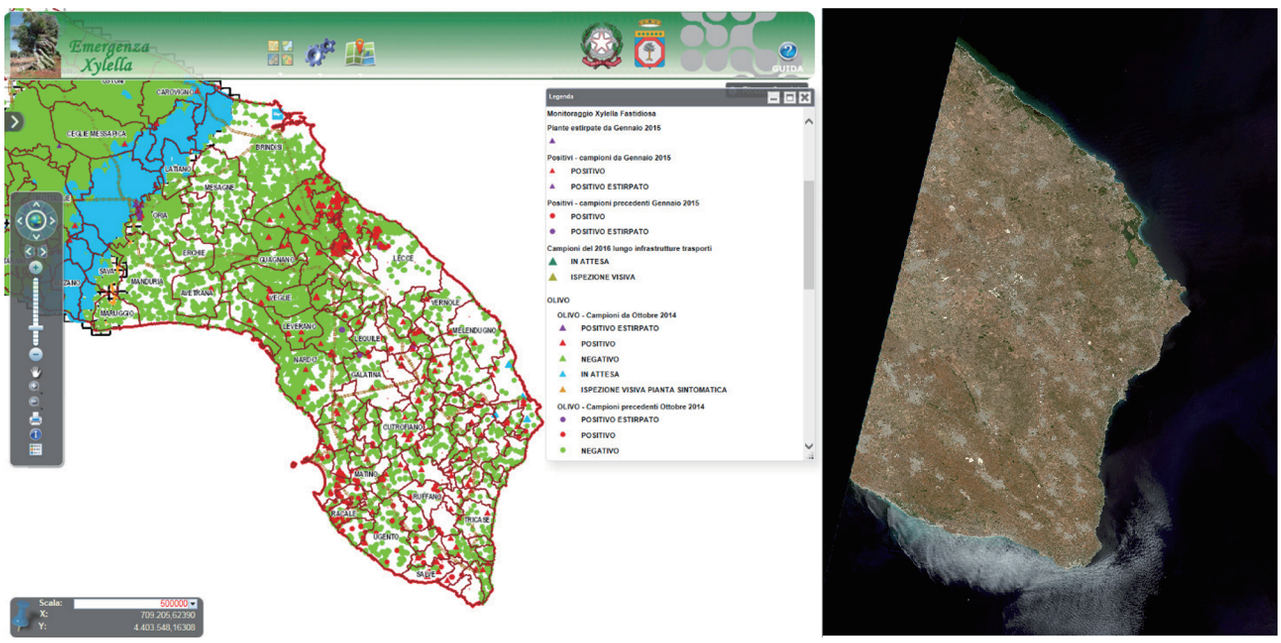

Fig.2 Distribution of the test sites (red triangles) analyzed, looking for the presence of the disease. On the right a Sentinel-2 image showing the area of interest considered in this paper.

2.1.2. Chinese test site

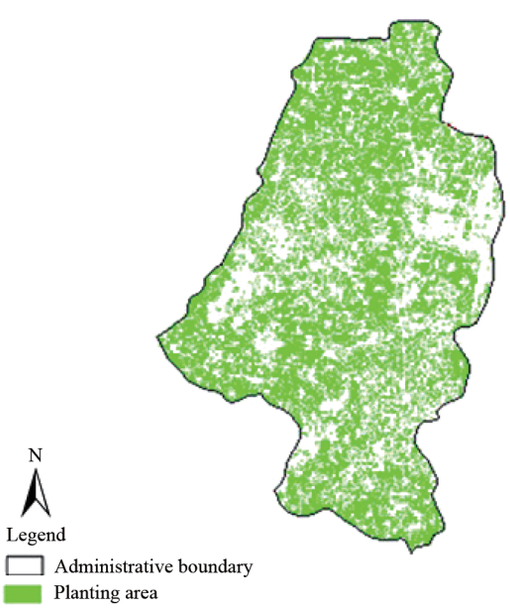

Fig.3 The location of the test site in Neihuang county, Henan province, China

To apply this approach an image segmentation is needed. The CLC 223 polygons has been segmented by using NDVI maps and a mathematical morphology approach [23-24]. Fig. 5 shows one of the images used with, superimposed, the CLC polygons corresponding to olive groves.

The procedure followed to segment the areas within the CLC polygons is schematically presented through the workflow of Fig. 5. Instead, Fig. 6 shows the procedure adopted to classify pixels in olive groves and not (see following paragraph.

(a) Google Earth, 19 July 2015 (b) Sentinel 2, 16 December 2016

Fig.4 Example of the variability of the land cover within a CLC class 223 polygon

The processing procedure has been implemented in Matlab [24]. The segmentation approach allows to identify similar areas but it is not intended to provide a classification of such areas. The classification is carried out by using an approach described in the following paragraphs. The results of the study are described in the following para-graph. The procedure foresees the following steps:

1. apply a segmentation function (gradient filter) to each CLC polygon;

2. Compute foreground markers(morphologic operators). These are connected blobs of pixels within each of the objects.

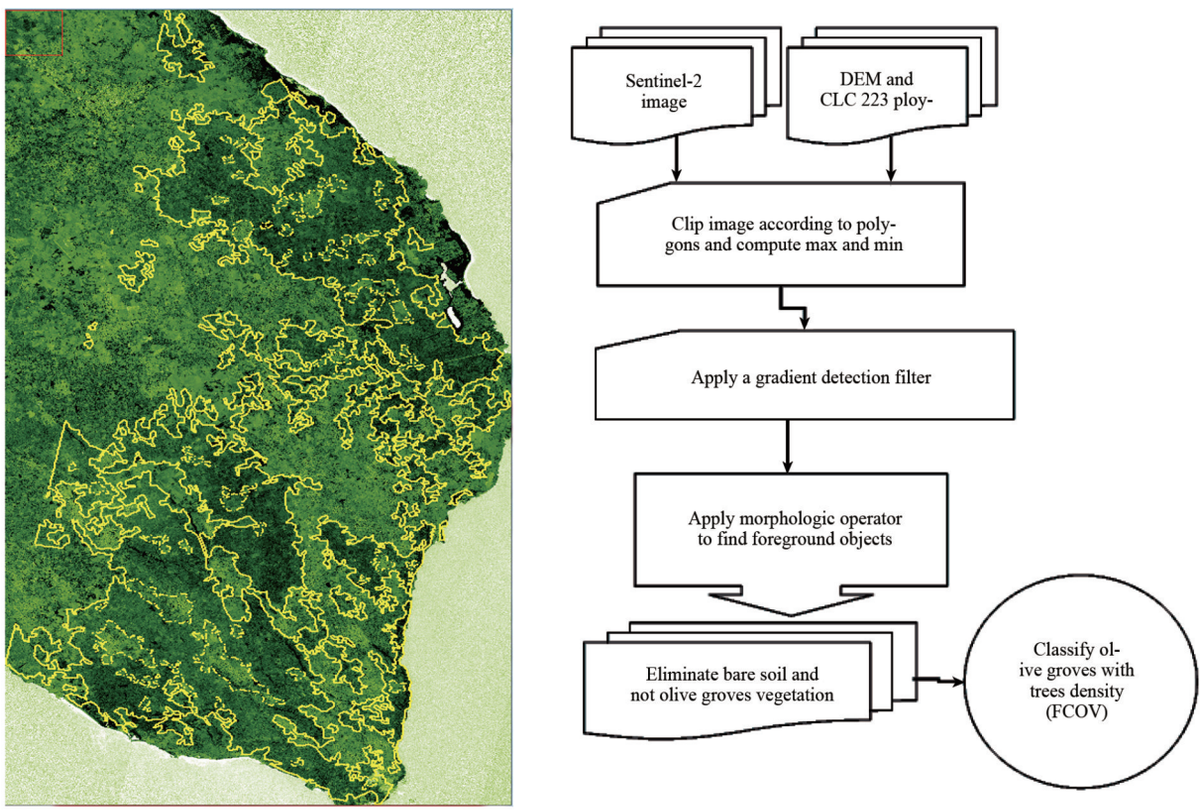

Fig.5 Left) Example of the NDVI distribution on the area considered in the study. Sentinel-2 image of the 14 July 2017. Right) Simplified workflow of the segmentation algorithm implemented in Matlab.

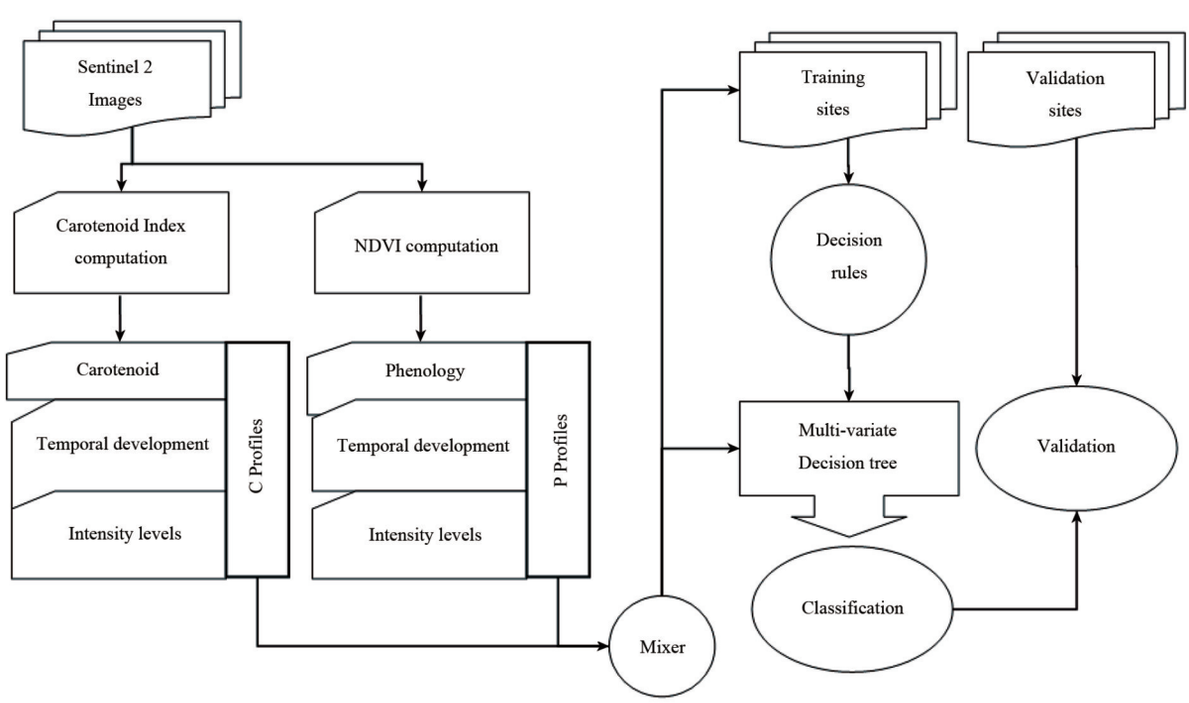

Fig.6 The final approach to the olive groves classification problem. New profiles, based on the evolution of the relation between carotenoid/chlorophyll content, are introduced. These profiles are mixed together with phenological data determining a new set of decision rules to be exploited by the MDT algorithm.

3. Using classification map based on time series of vegetation indices (see next paragraph) the polygons corresponding to olive groves are retained;

4. For each of these polygons max, min, average and standard

deviation of NDVI are computed;

5. Estimate FVC (Fraction of Vegetation Cover, that is the fraction of trees in each polygon).

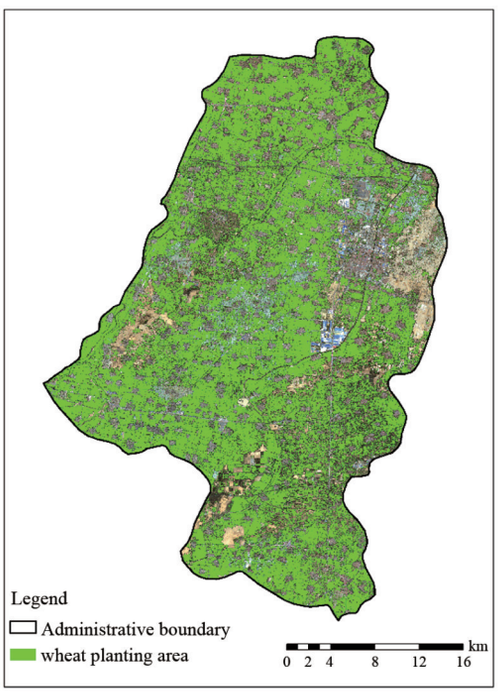

Fig.7 The extraction of winter wheat area of Neihuang county, Henan province of China.

Fig. 8 shows two examples of the results obtained by combining the NDVI based segmentation with the already available CLC polygons for olive groves.

2.2.1 Classification based on indices Olive groves

A multi-temporal phenology based classification algorithm was implemented to carry out the olive trees classification over the study area [25]. Sentinel 2 imagery was used over selected training sites to track olive trees characteristic evolution over a reference period of one year. Once the phenological development had been recognized, a multivariate decision tree was developed to classify the previously segmented areas. Although the aforementioned methodology had proven itself to be quite effective on highly populated olive tree orchards, an elevated number of sparsely populated olive trees areas was completely ignored by the algorithm. Missing areas are the result of the pixel contamination operated by the olive trees surrounding vegetation; because of that the olive trees phenological profile is highly deviating from the reference one. In order to overcome this drawback, we introduce the tracking of the vegetation carotenoid relative content with respect to chlorophyll, and we finally assessed the effectiveness of such a combined methodology by refining the classification land cover map which had previously been developed, for the province of Lecce, in the framework of the Corine project.

Phenological profiles analysis implies the detection and recognition of characteristic trends and growth/senescence stages in the yearly evolution of the vegetal species [26]. The NDVI is among the most widely used parameter in the tracking of vegetation seasonal trends and has been selected to investigate the timeline of the olive trees development in South-Italy. The temporal analysis is supported by the evaluation of the NDVIs' intensity related with the olive trees developmental stages by using a set of thresholds which were previously assessed over selected training sites.

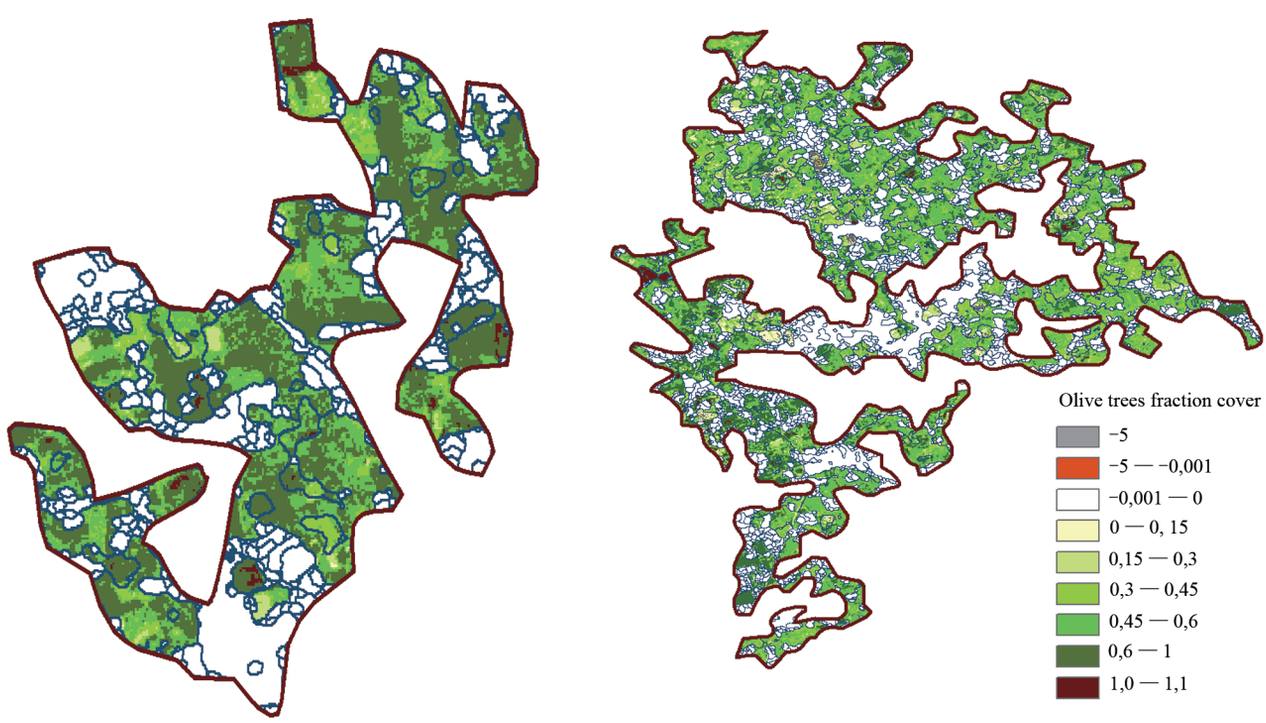

Fig.8 Details of the classification obtained by using vegetation index (green areas) compared with the one provided by Corine (red polygon). White regions in the Corine polygons correspond to areas in which less of the 80% of the surface is classified as olive groves. A qualitative estimate of the olive trees fraction cover, in each of the blue polygons obtained by image segmentation, is given. Areas with density values larger than 1 correspond to woodland/forest.

Among the parameters that characterized olive groves, the density of trees is the most important in order to operate a proper discrimination on texture basis. Highly populated olive groves are characterized by a texture which cannot be discriminated from the one showed by forest areas; on the other hand, medium to sparsely populated olive groves are characterized by a very specific and distinctive texture. The firsts can be effectively discriminated from forest areas and other kind of vegetation by using the here presented phenological approach alone; the same approach, on the other hand, it's not as much effective on the seconds because of the pixel spectral contamination due to the vegetation surrounding the olive trees. This spectral contamination manifest itself through the perturbation of the phenological profile by altering, and in particular increasing, the intensity levels. To support the phenological approach toward the resolution of the classification problem, the tracking of the carotenoid index was introduced.

The carotenoid reflectance measurement is sensitive to carotenoid pigments in plant leaves. The leaf carotenoid content estimation is much more difficult than chlorophyll estimation because of the overlap between carotenoid and chlorophyll absorption peaks. Usually the chlorophyll concentration is higher than carotenoid. The carotenoid reciprocal reflectance is maximal at 510 nm and this value is also influenced by chlorophyll. The reciprocal reflectance at 550 nm, which is more purely influenced by chlorophyll, is used to remove its effect on the measurement. A greater carotenoid concentration with respect to chlorophyll, is indicated by index higher values [27]. The evolution of the carotenoid content with respect to chlorophyll was then implemented into the main algorithm to make it keep scouting the residual areas searching for accorded variation through the growth/senescence stage of both the NDVI and the carotenoid index. Making the main algorithm capable of detecting low density olive groves, improves the effectiveness of the whole classification process; the workflow was then modified as showed in Fig.6

The proposed classification methodology allows to refine the previous land cover map developed in the framework of the Corine project, see next paragraph devoted to describe the results.

Wheat disease affected areas

Following the integration processing of hyperspectral data, an independent t-test was applied to examine the statistical significance of all bands based on healthy, slightly, and severely infected samples at the highest significance level (p-value < 0.001). We found that seven Sentinel-2 spectral bands (i.e., B3, B4, B5, B6, B7, B8, and B8a) manifested excellent potential for discriminating healthy and infected (slight and severe) samples (p-value < 0.001). According to the literature review, numerous SVIs (Spectral Vegetation Indexes) have been used to identify crop diseases. An independent t-test was used in this study to explore the significance of the SVIs related to the above seven bands, and the most significant (p-value < 0.001) SVIs were selected to identify yellow rust. Fig. 7 shows the distribution of winter wheat in the area of interest. These SVIs included conventional and red-edge vegetation indexes (as shown in Table 4). The conventional VIs, such as the NDVI, are often used to evaluate crop's growth state, and RGR has been used to estimate leaf pigments. GNDVI (Green Normalized Difference Vegetation Index) and $VARI_{green}$ (Visible Atmospherically Resistant Index) have been used to monitor crop disease. The red-edge VIs include the $NDVI_{Re1}$ which is similar to the NDVI but uses one of the red-edge bands (B5, B6, B7) instead of the red band (B4). NREDI is the index of normalized red-edge bands, and PSRI (Plant Senescence Reflectance Index) and ARI (Anthocyanin Reflectance Index) indicate crop physiological conditions and leaf pigments, respectively [28].

3 Results

The results, based on Sentinel-2 imagery, of the classification carried out as said above are summarized herein through Fig. 8 and the Table 3. Fig. 8 compares the olive groves polygons in CLC (class code 223) with those computed using our approach. Areas vegetated but not covered by olive trees (woodland, shrubland, etc.) are represented in marron (legend value 1.1). Table 3 describes the improvement obtained in the identification of olive groves with respect to the CLC classification map.

Table 3 Comparison between Corine classification and the new methodology described in the text.

Classification	Olive groves total extension/ha	Difference/ha	Difference/%
Corine (CLC)	78,982		
Dragon (Corine polygon)	56,642	−22,340	−28
Dragon (new areas)	103,801	+24,819	+23

The new methodology has been applied over the areas previously classified by Corine and, at the same time, over the whole geographic area covered by Corine, resulting in:

(1) reducing of the olive grove areas as proposed by Corine

(2) adding of new olive grove areas inside the covered area, and not previously classified by Corine

Table 3 shows the extent of the improvements to the land cover map with regard to olive groves achieved with the approach described above.

Now, for each of the polygons computed by using the segmentation based on mathematical morphology, using the classification map based on vegetation indices, we can:

(1) Assessing if the polygon cover an olive groves or winter wheat field;

(2) If pixels in the polygon are mainly appertaining to the class 'olive' (80 % pixels classified as olive groves) or 'winter wheat' we can proceed with estimating max, min, average and standard deviation of NDVI;

(3) Using the NDVI values for each polygon we can compute the FVC (or fraction of olive trees cover) in each polygon.

(4) Introducing an hypothesis on the olive trees size, from the previous, we can further counting the number of olive trees in each polygon.

Fig. 8 shows the olive trees density distribution in terms of pixel fraction cover (FVC) computed as said above. Only polygons covering an area larger than 2 ha have been considered. Pixels falling in polygons corresponding to olive groves and characterized by a different density distribution of trees, are represented in a colors scale. Five (Fig. 8) fraction cover levels are considered.

After that, having estimated the olive trees fraction cover and then the trees density (Fig. 9), we can attempt to assess the trees number by assigning an averaged size for each tree. For instance, assuming that olive trees have an averaged canopy diameter of 6 m we obtain the map shown in Fig. 10.

However, combining the classification based on Sentinel 2 images and VHR (Very High Resolution) images, a direct counting of the olive trees has been done. The watershed transform technique [31] has been used. The watershed transform finds "catchment basins" or "watershed ridge lines" in an image by treating it as a surface where light pixels represent high elevations and dark pixels

represent low elevations. If the topographical function is itself a distance function, then the topographical distance becomes identical with the geodesic distance function and the watershed becomes identical with the skeleton by zone of influence. This technique has been applied to the panchromatic image provided by the VHR sensor on board of the GF1 satellite. The results were compared with those obtained by applying the methodology based on FVC (Fraction of Vegetation Cover) to S2 images.

Table 4 Summary of spectral vegetation indexes used for detecting yellow rust (Sentinel 2 case).

SVIs	Definition	Formula
NDVI	Normalized difference vegetation index	$(R_{NLR}-R_R)/R_{NLR}+R_R$
EVI	Enhanced vegetation index	$2.5(R_{NLR}-R_R)/(R_{NLR}+6R_R-0.5R_B+1)$
RGR	Ration of red and green	R_R/R_G
$VARI_{green}$	Visible atmospherically resistant index	$(R_G-R_R)/R_G+R_R$
$NDVI_{Re1}$	Normalized difference vegetation index red-edge1	$*(R_{NLR}-R_{Rel})/R_{NLR}+R_{Rel}$
NREDI1	Normalized red-edge1 index	$(R_{Re2}-R_{Re1})/(R_{Re2}+R_{Re1})$
NREDI2	Normalized red-edge2 index	$(R_{Re3}-R_{Re1})/(R_{Re3}+R_{Re1})$
NREDI3	Normalized red-edge3 index	$(R_{Re3}-R_{Re2})/(R_{Re3}+R_{Re2})$
PSRI	Plant senescence reflectance index	$(R_R-R_G)/R_{Re1}$
REDSI	Red edge disease stress index	$**(705-665)\cdot(R_{Re3}-R_4)-(783-665)\cdot(R_{Re1}-R_4))/2\cdot R_4$

Note: * R_{Re1}, R_{Re2} R_{Re3} correspond to Sentinel-2 red-edge channels 5, 6 and 7, respectively** 665, 705, 783 represent the central wavelengths of the Sentinel 2 channel 4, 5 and 7.Random forest (RF) is an ensemble of learning algorithms. It assumes an original training set, and each instance with M attributes (M is the number of the feature dimensionality. In our case M=10 because we selected 10 vegetation indices as the RS descriptors of the wheat rust surface attributes). *m* is randomly selected in each computing node, in order to calculated the importance (weight) of each feature in the RF.. During the forest construction process, "Random" performs in two aspects: (1) It samples a new training set with replacement at each iteration, and the new training set is the same size as the original set; (2) Rather than choosing the best split among all attributes, m attributes are randomly chosen from M at each node and then these m attributes are used to split the node according to the principle of the decision tree algorithm, where m << M, and it is held constant during the forest construction process. Because the algorithm does not use all samples for model training at one time, this makes it possible to use the remaining samples (out of bag data) to evaluate the out of bag error (OOB error). Moreover, the principle of the feature importance ranking is to compare the difference in OOB error of each feature before and after adding noise to determine the importance of each feature. Thus, the importance of each feature is directly proportional to the difference. What we want is to reduce the original high-dimensional feature space, and improve the computing efficiency for real-time detection and classification of wheat rust. So, we do our best to filter the information in both the feature pre-selection stage or model training stage. We used the RF algorithm to calculate the importance ranking of features in our study. The more detailed information about our method had been reported in [28-30].

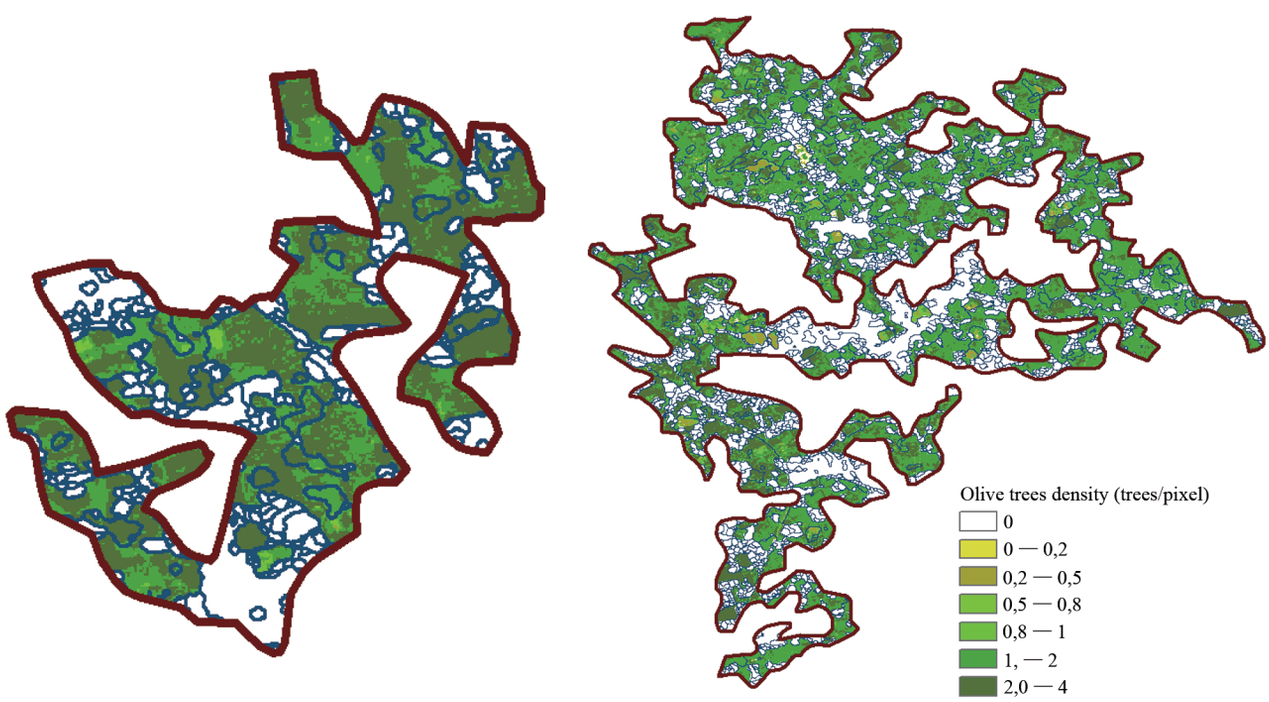

Fig.9 Example of the distribution of the density of olive trees computed as described in the text within two of the polygons corresponding to the class 223 (olive groves) of the Corine Land Cover.

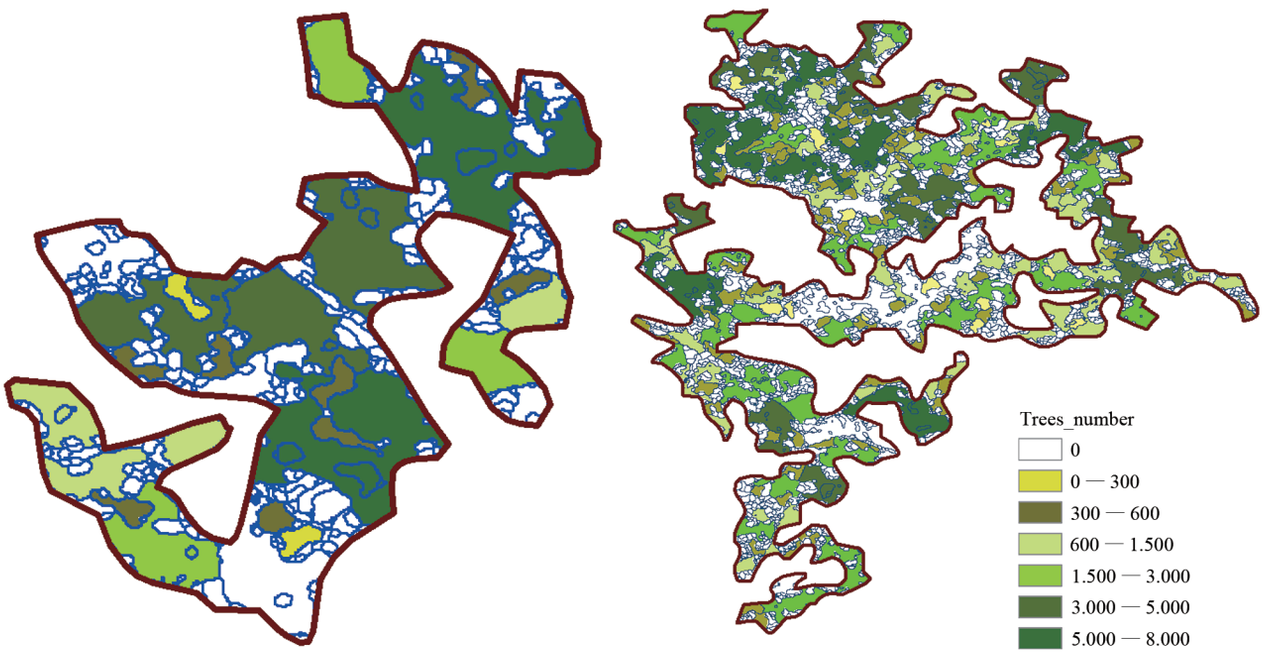

Fig.10 Example of the distribution of the total number of olive trees for each field computed as described in the text within two of the polygons corresponding to class 223 (olive groves) of the Corine Land Cover.

The validation of the results shown in Fig. 9 and Fig. 10 has been carried out by using VHR satellite images. Unfortunately, we were not able to fly on the area with our drone equipped with a multi-spectral camera (MicaSense-RedEdge sensor on board a UAV SkyRobotics-VTOL-SF6) due to a failure of the image-geolocation system. The VHR image we are referring to is the one provided by RADI acquired by the Chinese satellite GF-1. The sensor characteristics are given in Table 2.

The results of the validation are presented in Fig. 11. In particular, Fig. 11 (upper) shows provides a comparison between the trees density (trees/ha) computed using the two approaches described above. As it can be seen, the trees density computed by using an approach based on VHR image seems more stable with respect to the 98 olive groves considered. In several cases the approach based on FVC seems to overestimate the trees density. The reason of this behavior can be explained by using Fig. 11 (lower).

In fact, this figure, clear shows as FVC approach tends to overestimate the number of trees present in a field as the size of the field increases. This is due to the fact that, if some sparse vegetation (grass, scrub) is present this will con-tribute to the final value of FVC and the to the computation of the total number of olive trees in the field. This effect is as much as significant as the size of the field increases. However, for most of the fields the results are satisfactorily similar.

Fig. 12 demonstrates the spatial distribution of healthy and yellow-rust-infected winter wheat obtained using the threshold value of 59.7 based on REDSI. The yellow rust infection occurred in most of the area in the yellow rust infection spatial distribution map, especially in the northern part of the study area. The distribution of winter wheat infected with yellow rust was almost the same as the entire winter wheat planting area in the region, while the distribution of yellow rust infection was scattered in the remaining areas. Such a pattern of disease distribution is consistent with the actual occurrence of yellow rust in winter wheat in this region. The optimal threshold method for REDSI achieved good identification results at the regional scale with a kappa coefficient of 0.67 and an overall accuracy of 85.2%. Consequently, REDSI (based on Sentinel-2 MSI data) demonstrated its ability to identify winter wheat yellow rust infection at regional scale.

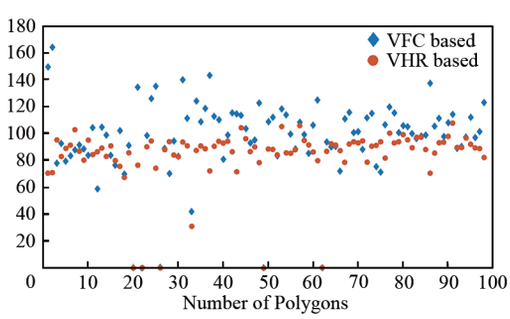

(a) Comparison between the trees density computed using VHR imagery and FVC on Sentinel-2 imag-es

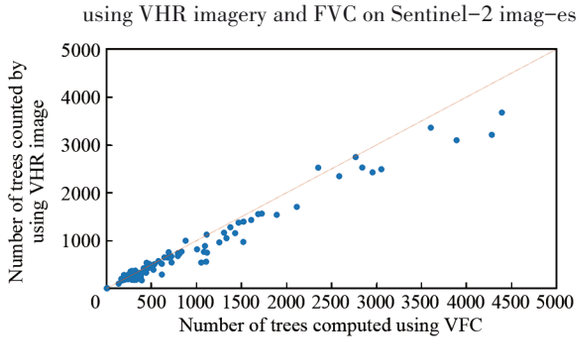

(b) Comparison of the total number of trees computed for each field by using VHR image and Sentinel 2 image

Fig.11

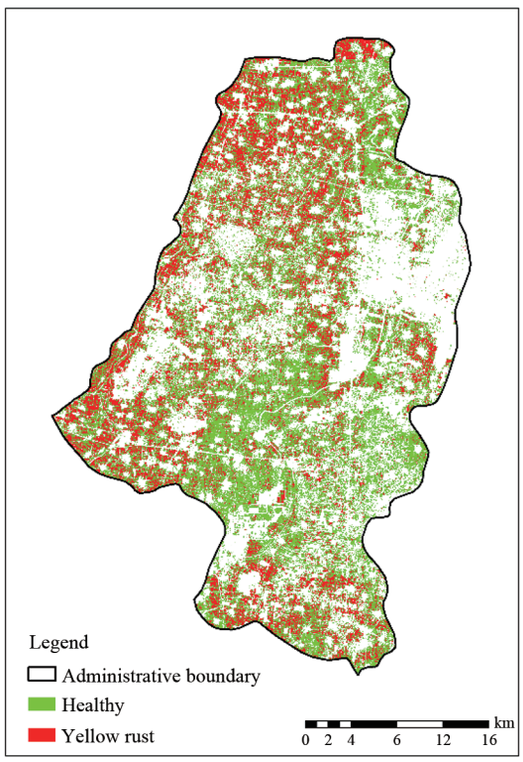

Fig.12 The occurrence distribution of the yellow rust in Neihuang county, Henan province of China.

4 Conclusions

The general objective of the AMEOS project is the delivery of information, based on assimilation of multi-sources satellite images, suitable to support the monitoring and forecast of insect pests and diseases in agriculture.

The specific objective of the two Chinese-Italian research groups regards the exploitation of available satellite images datasets to assess the evolution of diseases on winter wheat and permanent crops (olive groves, vineyards). In particular, in China the study concerns the monitoring of the yellow rust spread in winter wheat crop in the Neihuang county whereas, in Italy the study concerns the spread of phytosanitary threats as the Xylella fastidiosa (olive groves) [36].

The research activity on Xylella fastidiosa threats of olive groves follows three main approaches:

(1) Improving the classification of the agricultural areas devoted to olive trees, starting from what has been made available from the Corine Land Cover initiative;

(2) Developing an approach suitable to be automated for estimating trees by using Sentinel 2 images. This tool will be used to monitor the spread of pest.

(3) Developing an approach suitable to be automated for counting trees by using very high spatial resolution images in areas at high risk of infection.

This paper describes the results obtained in pursuing the first two approaches. In particular, the approach exploiting the characteristics olive tree phenology and carotenoid indices allowed to improve the classification of the olive groves in the area of interest with respect to the Corine Land Cover. Further, the use of a morphological approach on NDVI computed by using Sentinel-2 images of 2017 allowed to assess the olive groves density and trees number for each crop field. The quality of the results were validated by using a VHR image. The next step consist in carry out the same analysis on images acquired in previous years (2015 or 2016) in order to verify the possibly to monitor the decrease in the number of olive trees as a consequence of the spread of the xylella fastidiosa disease. The third point is still on-going as part of the activity of the PhD student funded by ESA.

The research activity on winter wheat disease used canopy hyperspectral data to simulate the corresponding multispectral bands of Sentinel-2, based on the relative spectral response (RSR) function of the Sentinel-2 multispectral sensor, and developed a new index, REDSI (consisting of Red, Re1, and Re3 bands), for detecting and monitoring yellow rust infection of winter wheat at the canopy and regional scale. Compared with other common spectral vegetation indexes, REDSI has excellent performance in detecting and monitoring yellow rust in winter wheat at the canopy and regional scale, with the overall accuracy of 84.1% and 85.2%, respectively. However, the index needs to be continually validated with other diseases and other cultivars to guide agriculture precision management.

References

Elbeaino T.; Yaseen T.; Valentini F.; Ben Moussa I. E.; Mazzoni V.; D'Onghia A.M. Identification of three potential insect vectors of Xylella fastidiosa in Southern Italy. Phytopathologia Mediterranea, 2014, 53(1), pp. 328 – 332.

Ben Moussa I.E.; Mazzoni V.; Valentini F.; Yaseen T.; Lorusso D.; Speranza S.; Digiaro M.; Varvaro L; Krugner R.; D'Onghia A.M. Seasonal Fluctuations of Sap-Feeding Insect Species Infected by Xylella fastidiosa in Apulian Olive Groves of Southern Italy. J. of Economic Entomology, 2016, 109(4), pp. 1512 – 1518.

Janse J.D.; Obradovic A. Xylella Fastidiosa: its biology, diagnosis, control and risks. J. of Plant Pathology, 2010, 92 (1, Supplement), pp. S1.35 – S1.48.

Dorigo W.; Zurita-Milla R.; de Wit A.J.; Brazile J.; Singh R.; Schaepman M.E. A review on reflective remote sensing and data assimilation techniques for enhanced agroecosystem modeling. Int. J. Appl. Earth Observ. Geoinf., 2007, 9(2), pp. 165 – 193.

Xie Q.; Huang W.; Dash J.; Song X.; Huang L.; Zhao J.; Wang R. Evaluating the potential of vegetation indices for winter wheat LAI estimation under different fertilization and water conditions. Adv. Space Res., 2015, 56(11), pp. 2365 – 2373.

Christou P.; Twyman R.M. The potential of genetically enhanced plants to address food insecurity. Nutrition Research Reviews, 2004, 17, pp. 23 – 42.

Strange R.N.; Scott P.R. Plant Disease: A Threat to Global Food Security. Annual review of Phytopathology, 2005, 40, pp. 83 – 116.

Huang W.; Luo J.; Zhang J.; Zhao J.; Zhao C.; Wang J.; Yang G.; Huang M.; Huang L.; Du S. Crop Disease and Pest Monitoring by Remote Sensing. In Remote Sensing Applications; Editor Boris Escalante, Intech: London, 2012, ISBN: 978-953-51-0651-7, Available online: https://www.intechopen.com/books/remote-sensing-applications/crop-disease-and-pest-monitoring-by-remote-sensing, (accessed on 31/08/2019.

Raikes C.; Burpee L.L. Use of multispectral radiometry for assessment of Rhizoctonia blight in creeping bentgrass. Phyto-pathology, 1998, 88, pp. 446-449.

Martinelli F.; Scalenghe R.; Davino S.; Panno S.; Scuderi G.; Panno s.; Scuderi G.; Ruisi P.; Villa P.; Stroppiana D.; Boschetti M.; Goulart L.R.; Davis C.E.; Dandekar A.M. Advanced methods of plant disease detection. A review. Agronomy for Sustainable Development, Springer Verlag/EDP Sciences/INRA, 2015, 35 (1), pp. 1-25. DOI 10.1007/s13593-014-0246-1.

Mahlein A.K.; Steiner U.; Hillnhutter C.; Dehne H.W.; Oerke E.C. Hyperspectral imaging for small-scale analysis of symptoms caused by different sugar beet diseases. Journal of Plant Methods, 2012, 8 (3, DOI 10.1186/1746-4811-8-3.

López-López M.; Calderón R.; González-Dugo V.; Zarco-Tejada P. J.; Fereres E. Early Detection and Quantification of Almond Red Leaf Blotch Using High-Resolution Hyperspectral and Thermal Imagery. Remote Sens., 2016, 8 (4, pp. 276.

Mahlein A. K.; Kuska M. T.; Thomas S.; Bohnenkamp D.; Alisaac E.; Behmann J.; Wahabzada M.; Kersting K. Plant disease detection by hyperspectral imaging: from the lab to the field, Advances in Animal Biosciences: Precision Agriculture (ECPA), 2017, 8(2), pp. 238 – 243.

Wang X.; Zhang M.; Zhu J.; Geng S. Spectral prediction of phytophthora infestants infection on tomatoes using artificial neural network (ANN). Int. J. Remote Sensing, 2008, 29, pp. 1693-1706.

Delalieux S.; van Aardt J.; Keulemans W.; Coppin P. Detection of biotic stress (Venturia inaequalis) in apple trees using hyperspectral data: non-parametric statistical approach and physiological implications. Eur. J. Agronomy, 2007, 27, pp. 130-143.

Beck P.S.A.; Zarco-Tejada P.; Strobl P.; San Miguel J. The feasibility of detecting trees affected by the Pine Wood Nematode using remote sensing. JRC Technical Report, 2015, DOI 10.2788/711975.

Mahlein A. K. Plant disease detection by imaging sensors – parallels and specific demands for precision agriculture and plant phenotyping. Plant Disease, 2016, 100(2), pp. 241-251.

AA.VV., Stimulating Scientific Exchange in Earth Observation Science and Technology, DRAGON 4 Cooperation, 2018, pp. 86-89, https: //indd. adobe. com/view/e8bcdb04-2d80-41cb-afcc-b4100b59f62c, (accessed on 31/08/2019.

Tucker C. J. Red and Photographic Infrared Linear Combinations for Monitoring Vegetation. Remote Sensing of Environment, 1979, 8 (2), pp. 127-150.

Genesis T.; Yengoh D.D.; Lennart O.; Tengberg A.E.; Tucker C.J. The use of the Normalized Difference Vegetation Index (NDVI) to assess land degradation at multiple scales: a review of the current status, future trends, and practical considerations. Lund University Center for Sustainability Studies (LUCSUS), and The Scientific and Technical Advisory Panel of the Global Environment Facility (STAP/GEF), 2014.

Diaz-Pacheco J.; Gutiérrez J. Exploring the limitations of CORINE Land Cover for monitoring urban land-use dynamics in metropolitan areas. Journal of Land Use Science, 2014, 9 (3), pp. 243 – 259.

Feranec J.; Hazeu G.; Christensen S.; Jaffrain G. Corine land cover change detection in Europe (case studies of the Netherland and Slovakia). Land Use Policy, 2007, 24(1), pp. 234 – 247.

Heijmans H. J. A. M.; Ronse C. The algebraic basis of mathematical morphology I. Dilations and Erosions. Computer Vision, Graphics, and Image Processing, 1990, 50(3), pp. 245 – 295.

Solomon C.; Breckon T. Fundamentals of Digital Image Processing: a practical approach with examples in MATLAB, Wiley-Blackwell, 2011.

Bradley B. A.; Mustard J. F. Comparison of phenology trends by land cover class: a case study in the Great Basin, USA. Global Change Biology, 2008, 14, pp. 334 – 346.

Aguilera F.; Fornaciari M.; Ruiz-Valenzuela L.; Galàn C, Msallem M.; Dhiab A.B.; Dìaz-de la Guardia C.; del Mar Trigo M.; Bonofiglio T.; Orlandi F. Phenological models to predict the main flowering phases of olive (Olea europaea L.) along a latitudinal and longitudinal gradient across the Mediterranean region. Int. J. Biometeorol, 2015, 59, pp. 629-641.

Gitelson A.; Zur Y.; Chivkunova O.; Merzlyak M.N. Assessing Carotenoid Content in Plant Leaves with Reflectance Spectroscopy¶. Photochemistry and photobiology, 2002, 75, pp. 272- 281.

Zheng Q.; Huang W.; Cui X.; Shi Y.; Liu L. New Spectral Index for Detecting Wheat Yellow Rust Using Sentinel-2 Multispectral Imagery, Sensors, 2018, 18(3), pp. 868-886.

Shi Y.; Huang W.; González-Moreno P.; Luke B.; Dong Y.; Zheng Q,; Ma H.; Liu L. Based Rust Spectral Feature Set (WRSFs): A Novel Spectral Feature Set Based on Continuous Wavelet Transformation for Tracking Progressive Host – Pathogen Interaction of Yellow Rust on Wheat, Remote Sensing, 2018, 10(4), pp. 525-543.

Shi Y. ; Huang W. ; Luo J. ; Huang L. ; Zhou X. Detection and discrimination of pests and diseases in winter wheat based on spectral indices and kernel discriminant analysis. Computers & Electronics in Agriculture, 2018, 141, pp. 171-180.

Meyer F. Topographic distance and watershed lines. Signal Processing, 1994, 38, pp. 113-125.